Impact of Cavity Geometry on Microlaser Dynamics

Kyungduk Kim,[1,*] Stefan Bittner,[2,3,*] Yuhao Jin,[4] Yongquan Zeng,[4] Qi Jie Wang,[4] and Hui Cao[1,†]
[1]Department of Applied Physics, Yale University, New Haven, Connecticut 06520, USA
[2]Université de Lorraine, CentraleSupélec, LMOPS, 2 rue Edouard Belin, Metz 57070, France
[3]Chair in Photonics, CentraleSupélec, LMOPS, 2 rue Edouard Belin, Metz 57070, France
[4]Center for OptoElectronics and Biophotonics, School of Electrical and Electronic Engineering, School of Physical and Mathematical Science, and Photonics Institute, Nanyang Technological University, 639798 Singapore

(Received 3 April 2023; accepted 8 September 2023; published 12 October 2023)

We experimentally investigate spatiotemporal lasing dynamics in semiconductor microcavities with various geometries, featuring integrable or chaotic ray dynamics. The classical ray dynamics directly impacts the lasing dynamics, which is primarily determined by the local directionality of long-lived ray trajectories. The directionality of optical propagation dictates the characteristic length scales of intensity variations, which play a pivotal role in nonlinear light-matter interactions. While wavelength-scale intensity variations tend to stabilize lasing dynamics, modulation on much longer scales causes spatial filamentation and irregular pulsation. Our results will pave the way to control the lasing dynamics by engineering the cavity geometry and ray dynamical properties.

DOI: 10.1103/PhysRevLett.131.153801

Controlling nonlinear dynamics of complex systems is crucial in, e.g., nonlinear optics, hydrodynamics, and laser physics [1,2]. It remains, however, a challenge to control semiconductor laser dynamics due to extremely fast inherent timescales [3]. Instead of relying on external feedback [4–8] or optical injection [9–12], we propose a more direct and compact approach based on modifying the intrinsic light-matter interaction inside the laser by tailoring the cavity geometry [13–15].

Broad-area Fabry-Perot cavities, commonly used for semiconductor lasers, often result in lasing instabilities [16–22]. An optical lensing effect in high-intensity regions, caused by spatial hole-burning and carrier-induced refractive index changes, leads to self-focusing of light and the formation of filaments, which are unstable and induce irregular pulsations. We recently showed that modifying the resonator shape can suppress spatiotemporal instabilities, e.g., in a D-shaped microcavity that features fully chaotic ray dynamics [13] or in a stable cavity with optimized mirror curvature that exhibits integrable ray dynamics [14,15]. The stability of lasing dynamics depends critically on the characteristic length scale of optical intensity variations in the cavity. If high-intensity regions, formed by constructive interference of propagating waves, are too small to induce a lensing effect, filamentation and lasing instability will be prevented. However, it is not clear how the cavity geometry affects the characteristic size of high-intensity regions and whether it is possible to predict the lasing dynamics based on classical ray dynamics.

To address these questions, we experimentally study how the classical ray dynamics is related to the spatiotemporal dynamics of semiconductor microcavity lasers. The ray dynamics of two-dimensional (2D) optical microcavities is entirely determined by the cavity shape and the boundary conditions. Hence, microlasers based on dielectric resonators correspond to billiards with (partial) ray escape according to Fresnel's laws [23,24]. Previously, the ray-wave correspondence was studied to reveal the relation between long-lived trajectories and resonances with high quality (Q) factors [24–28]. Most studies have concentrated on static properties like emission spectra and far-field distributions [29–34], except a few numerical [35,36] and experimental studies [13,37–40] of the dynamic properties of deformed microcavity lasers.

Here, we extend the paradigm of ray-wave correspondence to engineering the nonlinear lasing dynamics by utilizing classical ray dynamics. We judiciously choose several cavity shapes not only with distinct types of ray dynamics: chaotic vs integrable but, more importantly, with varying structural sizes and degrees of spatial localization of their lasing modes. We find the strength and occurrence of irregular pulsations of the laser emission are strongly correlated with the local structure size of the lasing modes, which are normally the most long-lived passive cavity resonances. This characteristic size is determined by the local directionality of optical propagation inside the cavity, which can be predicted by the classical ray dynamics.

Figure 1 shows five cavity geometries: D-cavity, stadium, Limaçon, ellipse, and square. These five shapes include cavities with chaotic (D-cavity, stadium, and Limaçon) and integrable (ellipse and square) ray dynamics. Furthermore, D-cavity, stadium, and square have spatially

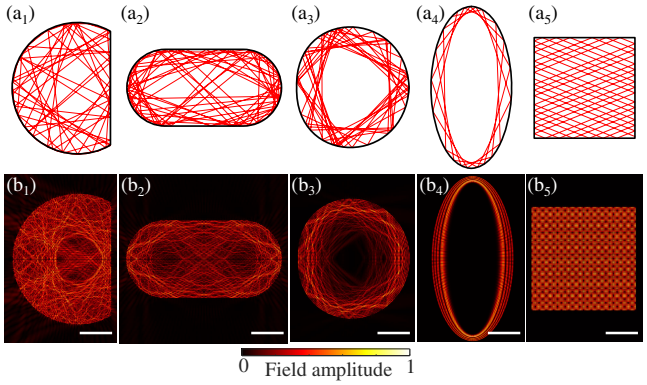

FIG. 1. Five cavity geometries with different classical ray dynamics. (a) Typical long-lived ray trajectories in D-shaped (a_1), stadium (a_2), Limaçon (a_3), ellipse (a_4), and square (a_5) dielectric cavities. (b) Numerically calculated mode profile with high Q factor in a cavity with a smooth boundary. The scale bars are 5 μm long.

extended modes featuring small structure size due to low local directionality of wave propagation, while Limaçon and ellipse have spatially localized whispering-gallery modes (WGMs) exhibiting large structure size due to directional wave propagation.

D-cavity and stadium have fully chaotic ray dynamics [41,42], and long-lived rays explore the bulk of the cavities [Figs. 1(a_1) and 1(a_2)]. Because of ray-wave correspondence [23,43–46], the high-Q modes are spatially extended and irregularly structured [Figs. 1(b_1) and 1(b_2)]. The Limaçon-shaped cavity features predominantly chaotic ray dynamics [47–49] but has long-lived trajectories concentrated at the cavity boundary [Fig. 1(a_3)], resulting in irregular WGMs [Fig. 1(b_3)]. The ellipse features integrable ray dynamics [50] with long-lived trajectories along the cavity boundary that are confined by total internal reflection [Fig. 1(a_4)], resulting in regularly structured WGMs [Fig. 1(b_4)]. The square also features integrable ray dynamics, but its long-lived trajectories explore the whole cavity [Fig. 1(a_5)], and, hence, its high-Q resonances [51–53] are spatially extended with regular, fine features [Fig. 1(b_5)].

We fabricate edge-emitting semiconductor microlasers with these five resonator shapes [54]. The devices are fabricated on a commercial laser diode wafer with a GaAs/AlGaAs quantum well (Q-Photonics QEWLD-808) by photolithography and inductively coupled plasma etching, followed by deposition of a top metal contact for electric current injection. Multiple cavities for each of the five geometries, with identical cavity areas (2.53×10^4 μm^2), are fabricated on the same wafer.

We study their spatiotemporal lasing dynamics experimentally using a streak camera (Hamamatsu C5680/M5676) to record the time-resolved near-field emission intensity profiles. We measure 10-ns-long time windows with a resolution of ∼30 ps. Lasing occurs in all cavities with electrical pumping at room temperature [54]. Figure 2(a) shows exemplary streak images. The spatial profiles of emission intensity agree with the output patterns of high-Q resonances [40,57]. The irregular pulsations with typical periods of subnanoseconds are caused by unstable lasing dynamics.

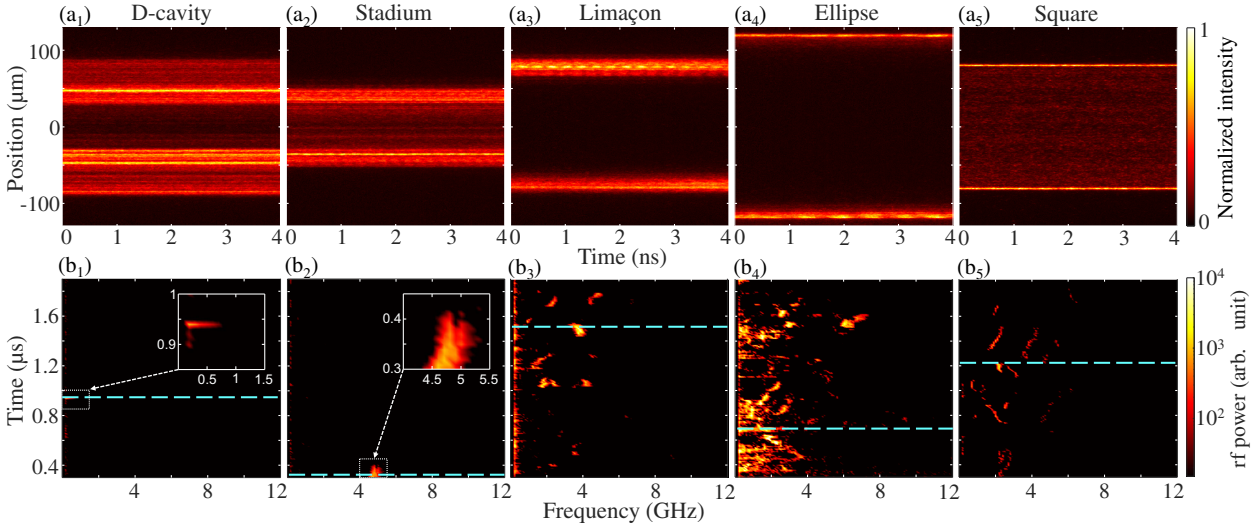

FIG. 2. Experimentally measured spatiotemporal lasing dynamics. (a_1)–(a_5) Streak images of lasing emission from five different cavity geometries. The intensity is normalized by its maximum. The pump current is 500 mA for all cavities, well above their lasing thresholds. Intensity pulsations indicate unstable lasing dynamics. (b_1)–(b_5) Time-resolved rf spectra $\hat{S}(f, t_d)$ of laser emission intensities obtained from the streak images. Insets in (b_1) and (b_2) are the magnifications of the white boxes. The cyan dashed lines indicate the times of the images in (a). rf peaks (bright spots) correspond to intensity pulsations.

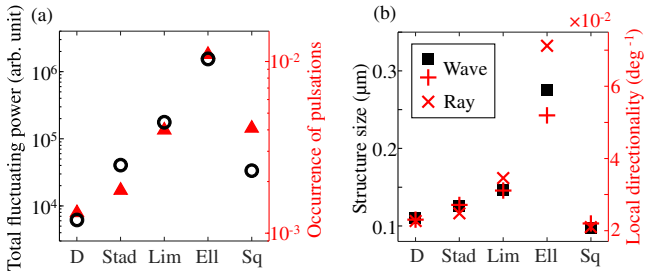

FIG. 3. Relation between lasing instabilities and spatial structure of lasing modes. (a) Experimentally measured total rf power S_{tot} of intensity pulsations (black circles, left axis) and the frequency of their occurrence (red triangles, right axis) for different cavity shapes. The results of five lasers per geometry are averaged on a logarithmic scale. (b) Numerically calculated local structure size $\langle s \rangle$ in five cavities with boundary roughness, averaged over the cavity area (black squares, left axis). It is determined by the local directionality of light propagation $\langle D_W \rangle$ and $\langle D_R \rangle$ (red symbols, right axis), obtained from wave (+) and ray simulations (×).

We analyze the laser intensity fluctuations using the short-term radio-frequency (rf) spectra and their temporal evolution. We calculate the temporal Fourier transform of every 10-ns-long streak image and average its magnitude squared in space. Then a broadband continuous signal from the spatiotemporal beating of lasing modes and amplified spontaneous emission is subtracted from the rf spectra, which highlights discrete peaks from irregular pulsations due to lasing instabilities [54]. The subtracted rf spectra in Figs. 2(b_1)–2(b_5) clearly show different degrees of stability for the five geometries.

For a more quantitative statistical analysis, we characterize the rf spectra with two measures in Fig. 3(a). The first one (left axis) is the total rf power S_{tot}, obtained by integrating the short-term rf spectra [Fig. 2(b)] in both frequency and time. The second one (right axis) measures the frequency of occurrence of rf peaks by the participation ratio of the rf spectra [54]. To account for the cavity-to-cavity variations, we average these quantities over five different lasers per geometry. Both the overall fluctuation power and the occurrence of intensity pulsations vary by several orders of magnitude for different cavity geometries. The D-cavity microlasers have the weakest and rarest pulsations, followed by the stadia. Limaçon cavities have stronger and more frequent pulsations than D-cavities and stadia. The ellipse lasers have the strongest and most frequent pulsations. The square cavities, in contrast, are much more stable than ellipses and close to stadia.

The spatial structure of the lasing modes strongly influences the nonlinear interaction between the optical field and gain material, which, in turn, affects the strength and occurrence of irregular pulsations. To reveal the underlying mechanism, we numerically characterize the fine structure of the lasing modes. We calculate the passive resonances of 2D cavities with boundary roughness to account for fabrication defects [54]. The cavity dimensions are 10 times smaller than the actual ones to reduce computational load. Furthermore, we employ steady-state *ab initio* lasing theory with single-pole approximation to determine which cavity resonances will lase and to calculate their lasing intensities [54,58–61].

The mode profiles in Fig. 4(b) show significant differences in their fine structure for the different geometries. The D-cavities and stadia [Figs. 4(b_1) and 4(b_2)] show random and isotropic intensity variations on the scale of the in-medium wavelength. For the Limaçon [Fig. 4(b_3)], in contrast, the fine structure is anisotropic with elongated high-intensity grains. This anisotropy is even more pronounced for the ellipses [Fig. 4(b_4)]. In contrast, the squares [Fig. 4(b_5)] feature a more regular structure with a feature size similar to that of D-cavities or stadia.

To characterize the typical size of the fine structure, we compute the spatial intensity correlation functions of high-Q resonances in a local area [54]. The contour lines at half maximum of the intensity correlation functions [blue dashed lines in Fig. 4(c)] are fitted by an ellipse [red solid lines in Fig. 4(c)]. While the length of the minor axis is consistent for all cavity shapes, the major axis of the ellipse varies significantly with the cavity geometry, and it is defined as the local structure size $s(\vec{r})$.

We calculate the average structure size $\langle s \rangle$ by first averaging over all lasing modes weighted by their intensities and then averaging over all spatial locations weighted by local intensity [54]. Figure 3 shows that $\langle s \rangle$ [Fig. 3(b), left axis] is strongly correlated with the lasing instabilities in the experiment [Fig. 3(a)]. The irregular pulsations of broad-area semiconductor lasers originate from carrier-induced modulational instability. In a GaAs quantum well, high optical intensity depletes the local gain by spatial hole burning, which increases the refractive index locally. The resulting optical lensing effect and self-focusing lead to the formation of spatial filaments, which are inherently unstable and cause pulsations [17–19]. For cavities with $\langle s \rangle \sim \lambda$, intensity variation on a wavelength scale causes a refractive index change on the same scale, which is too small to focus light [13], thus preventing filamentation and instability. Conversely, a large feature size $\langle s \rangle \gg \lambda$ is more likely to create a lensing effect, which leads to stronger and more frequent pulsations. Therefore, the structure size appears to be a good predictor for the level of lasing stability.

The question is what determines the local structure size of lasing modes. The granular structure of lasing modes is formed by the interference of waves propagating in different directions. Thus, the distribution of their directions plays a significant role, which can be unraveled by the spatial Fourier transform of the field profiles. Since it is the *local* directionality that determines the structure size of the intensity distributions, we determine the wave

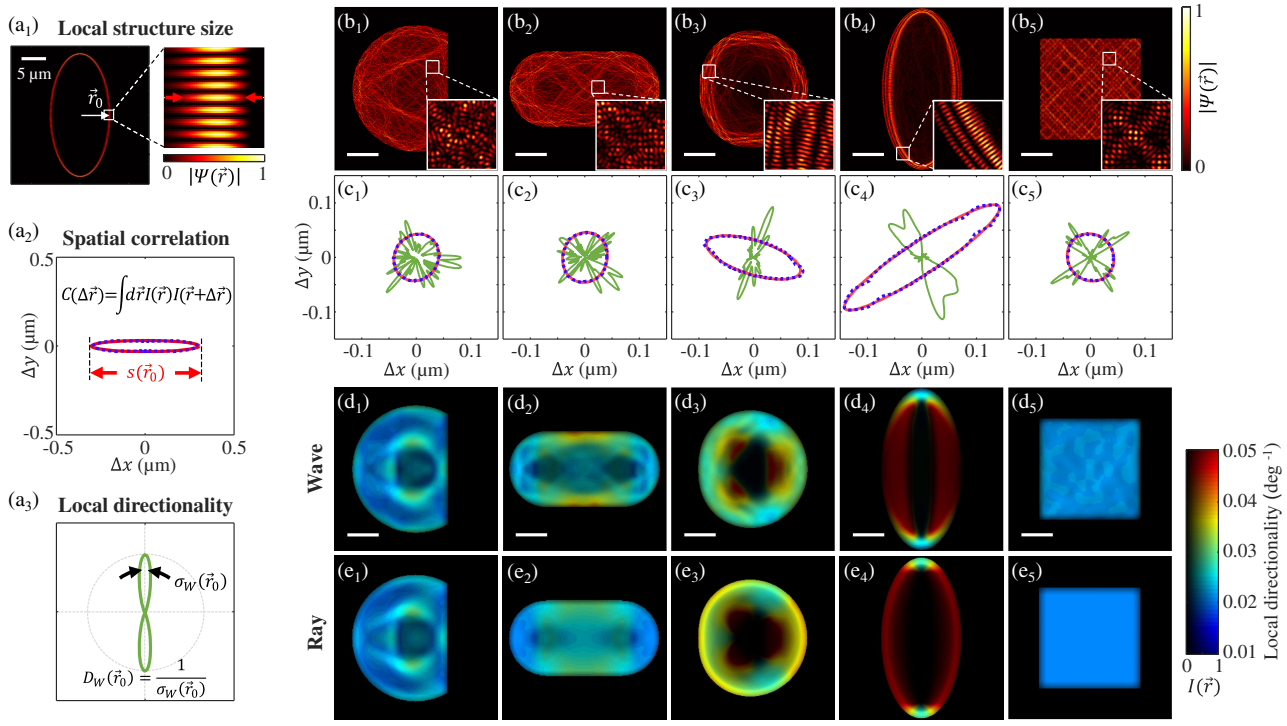

FIG. 4. Numerically simulated local directionality of optical propagation. (a_1)–(a_3) Illustration of local structure size and local directionality. (a_1) An exemplary high-Q mode in an elliptic cavity features highly directional optical propagation, which yields elongated bright regions. The red arrows denote the structure size. (a_2) The half-maximum contour line of the spatial intensity correlation function $C(\Delta\vec{r})$ (blue dotted lines) for the white box centered at $\vec{r}_0$ in (a_1). It is fitted by an ellipse (solid red line) whose major axis is equal to the elongated feature size in (a_1) and defines the local structure size of 0.6 μm (red arrows). (a_3) Polar plot of the amplitude of local Fourier component $|w_\mu(\vec{r}_0,\theta)|$ (green), obtained by wavelet transform at the center $\vec{r}_0$ of the white box in (a_1). The standard deviation of its amplitude squared is 6.7° (black arrows), whose inverse yields the local directionality. (b_1)–(b_5) Typical high-Q modes of five cavity shapes with surface roughness. The scale bars are 5 μm long. Insets: magnifications of the white boxes. (c_1)–(c_5) The analysis illustrated in (a) is performed with the modes in (b). (d_1)–(d_5) Maps of local directionality $D_W(\vec{r})$ of the simulated lasing modes. The color denotes the local directionality (red, high; blue, low), and the brightness denotes the local intensity of lasing modes. (e_1)–(e_5) Map of local directionality $D_R(\vec{r})$ obtained from ray tracing, showing excellent agreement with wave simulations in (d).

propagation directions in small regions by performing a wavelet transform [62], which can be considered as a local Fourier transform [green solid lines in Fig. 4(c)] [54]. The local directionality is defined as the inverse of the angular spread of wavelet distributions [Fig. 4(a)]. The D-cavities and stadia [Figs. 4(c_1)–4(c_2)] show wave propagation along almost all directions. The interference of these wave components yields a small structure size. For the Limaçon with WGMs [Fig. 4(c_3)], the distribution of wave propagation is more directional parallel to the cavity boundary, leading to a larger structure size perpendicular to the boundary. The ellipses [Fig. 4(c_4)] exhibit a smooth and highly directional distribution, which explains the significantly elongated fine structure of their intensity distributions. Lastly, the square [Fig. 4(c_5)] features four double-peaked lobes along the diagonals, which correspond to the eight plane-wave components of high-Q modes [51,52]. Despite the low number of plane-wave components, their interference produces nearly isotropic, wavelength-scale intensity grains, because the propagation directions are roughly orthogonal.

To quantify how directional the wave propagation is in a local area, we compute the local directionality $D_W(\vec{r})$ as the inverse of the standard deviation of the wavelet distribution squared [54]. Figure 4(d) shows the spatially resolved directionality $D_W(\vec{r})$, averaged over the lasing modes. The D-shaped and stadium cavities [Figs. 4(d_1) and 4(d_2)] have lower $D_W(\vec{r})$ than Limaçon resonators [Fig. 4(d_3)], which demonstrates the difference between spatially extended and whispering-gallery modes. The local directionality of the ellipses [Fig. 4(d_4)] is even higher than for the Limaçon, probably due to the integrable ray dynamics of the ellipse, which limits the propagation directions of whispering-gallery trajectories more than for the chaotic trajectories of the Limaçon. The squares [Fig. 4(d_5)] have low and almost uniform $D_W(\vec{r})$ over the cavity area.

These different degrees of local directionality originate from the classical ray dynamics. We, hence, perform ray tracing simulations for cavities with smooth boundaries and define the local directionality $D_R(\vec{r})$ analogously by sampling the long-lived ray trajectories [54]. Figure 4(e) shows an excellent agreement between the ray and wave

simulations. We average the local directionality over the entire cavity area weighted by the ray intensity, and the results are summarized in Fig. 3(b) (right axis). The good agreement of local directionality between ray $\langle D_R \rangle$ and wave simulations $\langle D_W \rangle$ indicates that a cavity with sufficiently small boundary roughness can be efficiently simulated by the ray tracing of smooth cavities. More importantly, the strong correlation between $\langle D_R \rangle$ and $\langle s \rangle$ confirms that the structure sizes of lasing modes are determined by the local directionality of optical propagation. Hence, our results demonstrate that ray dynamics can be an efficient tool to qualitatively predict the spatiotemporal lasing dynamics.

Apart from the structure size of lasing modes, spatial localization of the modes can also promote the nonlinear processes in the gain medium. Cavities with WGMs like Limaçon or ellipse feature high local optical intensities, and this may facilitate the self-focusing effect and result in stronger output intensity pulsations. Even though simulations with a detailed model of semiconductor carrier dynamics for asymmetric cavities are desirable for a full understanding, our analysis of experiments and passive cavity modes already yields important insights into the relation between the spatial structure of cavity modes and nonlinear lasing dynamics.

In conclusion, we establish the resonator geometry as a powerful design parameter to control the spatiotemporal dynamics of semiconductor microlasers. The lasing dynamics is related to the local directionality of wave propagation, which directly corresponds to the ray dynamics. Our findings enable us to engineer the lasing dynamics by designing the cavity shape based on ray-dynamical principles. In contrast to the design of chaotic microlasers by tailoring temporal oscillation frequencies [39,63], our approach is based on tailoring the spatial frequencies of lasing modes, which provides a huge and unexplored parameter space. From a practical perspective, customizing the cavity shape enables compact devices to be easily integrated on chip, in contrast to optical injection and time-delayed feedback [3,64,65]. Potential applications are the development of high-power broad-area lasers with stable dynamics and compact lasers for chaos-based applications [65,66]. Furthermore, the principle of controlling the nonlinear dynamics via its geometry can also find application in other types of lasers such as broad-area vertical-cavity surface-emitting lasers [67–69] or random lasers [70], as well as in other nonlinear dynamic systems in aerodynamics, fluid dynamics, and plasma physics.

The authors thank Roland Ketzmerick, Jan Wiersig, Ortwin Hess, Stefano Guazzotti, Takahisa Harayama, and Douglas Stone for fruitful discussions. H. C. and K. K. acknowledge the computational resources provided by the Yale High Performance Computing Cluster (Yale HPC). The work done at Yale is supported partly by the National Science Foundation under Grant No. ECCS-1953959 and the Office of Naval Research under Grant No. N00014-221-1-2026. S. B. acknowledges funding for the Chair in Photonics by Ministère d'Enseignement Supérieur et de la Recherche (France); GDI Simulation; Région Grand-Est; Département Moselle; European Regional Development Fund (ERDF); CentraleSupélec; Fondation CentraleSupélec; and Metz Metropole. Q. J. Wang, Y. J., and Y. Z. acknowledge National Research Foundation Competitive Research Program (NRF-CRP19-2017-01) and National Medical Research Council (NMRC) MOH-000927.

*These authors contributed equally to this work.
†hui.cao@yale.edu

[1] E. Ott, C. Grebogi, and J. A. Yorke, Controlling Chaos, Phys. Rev. Lett. **64**, 1196 (1990).
[2] R. Roy, T. Murphy Jr, T. Maier, Z. Gills, and E. Hunt, Dynamical Control of a Chaotic Laser: Experimental Stabilization of a Globally Coupled System, Phys. Rev. Lett. **68**, 1259 (1992).
[3] J. Ohtsubo, *Semiconductor Lasers—Stability, Instability and Chaos*, 3rd ed. (Springer, Heidelberg, 2013).
[4] J. Mørk, J. Mark, and B. Tromborg, Route to Chaos and Competition between Relaxation Oscillations for a Semiconductor Laser with Optical Feedback, Phys. Rev. Lett. **65**, 1999 (1990).
[5] I. Fischer, O. Hess, W. Elsäßer, and E. Göbel, High-Dimensional Chaotic Dynamics of an External Cavity Semiconductor Laser, Phys. Rev. Lett. **73**, 2188 (1994).
[6] I. Fischer, G. Van Tartwijk, A. Levine, W. Elsäßer, E. Göbel, and D. Lenstra, Fast Pulsing and Chaotic Itinerancy with a Drift in the Coherence Collapse of Semiconductor Lasers, Phys. Rev. Lett. **76**, 220 (1996).
[7] J. Martin-Regalado, G. Van Tartwijk, S. Balle, and M. San Miguel, Mode control and pattern stabilization in broad-area lasers by optical feedback, Phys. Rev. A **54**, 5386 (1996).
[8] S. K. Mandre, I. Fischer, and W. Elsäßer, Spatiotemporal emission dynamics of a broad-area semiconductor laser in an external cavity: Stabilization and feedback-induced instabilities, Opt. Commun. **244**, 355 (2005).
[9] S. Wieczorek, B. Krauskopf, and D. Lenstra, A unifying view of bifurcations in a semiconductor laser subject to optical injection, Opt. Commun. **172**, 279 (1999).
[10] S. Hwang and J. Liu, Dynamical characteristics of an optically injected semiconductor laser, Opt. Commun. **183**, 195 (2000).
[11] B. Krauskopf, S. Wieczorek, and D. Lenstra, Different types of chaos in an optically injected semiconductor laser, Appl. Phys. Lett. **77**, 1611 (2000).
[12] S. Takimoto, T. Tachikawa, R. Shogenji, and J. Ohtsubo, Control of spatio-temporal dynamics of broad-area semiconductor lasers by strong optical injection, IEEE Photonics Technol. Lett. **21**, 1051 (2009).
[13] S. Bittner, S. Guazzotti, Y. Zeng, X. Hu, H. Yılmaz, K. Kim, S. S. Oh, Q. J. Wang, O. Hess, and H. Cao, Suppressing spatio-temporal lasing instabilities with wave-chaotic microcavities, Science **361**, 1225 (2018).

[14] K. Kim, S. Bittner, Y. Zeng, S. Guazzotti, O. Hess, Q. J. Wang, and H. Cao, Massively parallel ultrafast random bit generation with a chip-scale laser, Science **371**, 948 (2021).
[15] K. Kim, S. Bittner, Y. Jin, Y. Zeng, S. Guazzotti, O. Hess, Q. J. Wang, and H. Cao, Sensitive control of broad-area semiconductor lasers by cavity shape, APL Photonics **7**, 056106 (2022).
[16] I. Fischer, O. Hess, W. Elsäßer, and E. Göbel, Complex spatio-temporal dynamics in the near-field of a broad-area semiconductor laser, Europhys. Lett. **35**, 579 (1996).
[17] O. Hess and T. Kuhn, Maxwell-bloch equations for spatially inhomogeneous semiconductor lasers. II. Spatiotemporal dynamics, Phys. Rev. A **54**, 3360 (1996).
[18] J. Marciante and G. Agrawal, Spatio-temporal characteristics of filamentation in broad-area semiconductor lasers, IEEE J. Quantum Electron. **33**, 1174 (1997).
[19] J. R. Marciante and G. P. Agrawal, Spatio-temporal characteristics of filamentation in broad-area semiconductor lasers: experimental results, IEEE Photonics Technol. Lett. **10**, 54 (1998).
[20] A. Klaedtke and O. Hess, Ultrafast nonlinear dynamics of whispering-gallery mode micro-cavity lasers, Opt. Express **14**, 2744 (2006).
[21] D. Scholz, H. Braun, U. T. Schwarz, S. Brüninghoff, D. Queren, A. Lell, and U. Strauss, Measurement and simulation of filamentation in (Al,In)GaN laser diodes, Opt. Express **16**, 6846 (2008).
[22] M. Arahata and A. Uchida, Inphase and antiphase dynamics of spatially-resolved light intensities emitted by a chaotic broad-area semiconductor laser, IEEE J. Sel. Top. Quantum Electron. **21**, 1800609 (2015).
[23] E. G. Altmann, J. S. E. Portela, and T. Tél, Leaking chaotic systems, Rev. Mod. Phys. **85**, 869 (2013).
[24] H. Cao and J. Wiersig, Dielectric microcavities: Model systems for wave chaos and non-Hermitian physics, Rev. Mod. Phys. **87**, 61 (2015).
[25] R. K. Chang and A. J. Campillo, *Optical Processes in Microcavities*, Vol. 3 (World Scientific, Singapore, 1996).
[26] A. D. Stone, Wave-chaotic optical resonators and lasers, Phys. Scr. **2001**, 248 (2001).
[27] H. E. Türeci, H. G. L. Schwefel, P. Jacquod, and A. D. Stone, Modes of wave-chaotic dielectric resonators, Prog. Opt. **47**, 75 (2005).
[28] T. Harayama and S. Shinohara, Two-dimensional microcavity lasers, Laser Photonics Rev. **5**, 247 (2011).
[29] A. Levi, R. Slusher, S. McCall, J. Glass, S. Pearton, and R. Logan, Directional light coupling from microdisk lasers, Appl. Phys. Lett. **62**, 561 (1993).
[30] J. U. Nöckel, A. D. Stone, G. Chen, H. L. Grossman, and R. K. Chang, Directional emission from asymmetric resonant cavities, Opt. Lett. **21**, 1609 (1996).
[31] G. Chern, H. Tureci, A. D. Stone, R. Chang, M. Kneissl, and N. Johnson, Unidirectional lasing from InGaN multiple-quantum-well spiral-shaped micropillars, Appl. Phys. Lett. **83**, 1710 (2003).
[32] H. G. L. Schwefel, H. E. Tureci, A. D. Stone, and R. K. Chang, Progress in asymmetric resonant cavities: Using shape as a design parameter in dielectric microcavity lasers, *Optical Processes in Microcavities* (World Scientific, Singapore, 2003).
[33] H. G. L. Schwefel, N. B. Rex, H. E. Tureci, R. K. Chang, A. D. Stone, T. Ben-Messaoud, and J. Zyss, Dramatic shape sensitivity of directional emission patterns from similarly deformed cylindrical polymer lasers, J. Opt. Soc. Am. B **21**, 923 (2004).
[34] T. Fukushima, T. Tanaka, and T. Harayama, Unidirectional beam emission from strained InGaAsP multiple-quantum-well quasistadium laser diodes, Appl. Phys. Lett. **86**, 171103 (2005).
[35] S. Sunada, T. Harayama, and K. S. Ikeda, Multimode lasing in two-dimensional fully chaotic cavity lasers, Phys. Rev. E **71**, 046209 (2005).
[36] T. Harayama, T. Fukushima, S. Sunada, and K. S. Ikeda, Chaos and multi-attractors in fully chaotic 2D microcavity lasers, Prog. Theor. Phys. Suppl. **166**, 104 (2007).
[37] M. Choi, T. Fukushima, and T. Harayama, Alternate oscillations in quasistadium laser diodes, Phys. Rev. A **77**, 063814 (2008).
[38] S. Shinohara, T. Fukushima, S. Sunada, T. Harayama, K. Arai, and K. Yoshimura, Anticorrelated bidirectional output of quasistadium-shaped semiconductor microlasers, Opt. Rev. **21**, 113 (2014).
[39] C.-G. Ma, J.-L. Xiao, Z.-X. Xiao, Y.-D. Yang, and Y.-Z. Huang, Chaotic microlasers caused by internal mode interaction for random number generation, Light: Sci. Appl. **11**, 187 (2022).
[40] K. Kim, S. Bittner, Y. Jin, Y. Zeng, Q. Wang, and H. Cao, Spatiotemporal lasing dynamics in a Limaçon-shaped microcavity, Opt. Lett. **48**, 574 (2023).
[41] L. A. Bunimovich, On the ergodic properties of nowhere dispersing billiards, Commun. Math. Phys. **65**, 295 (1979).
[42] S. Ree and L. E. Reichl, Classical and quantum chaos in a circular billiard with a straight cut, Phys. Rev. E **60**, 1607 (1999).
[43] M. V. Berry, Regular and irregular semiclassical wavefunctions, J. Phys. A **10**, 2083 (1977).
[44] A. I. Shnirel'man, Ergodic properties of eigenfunctions, Usp. Mat. Nauk **29**, 181 (1974).
[45] R. Ketzmerick, K. Clauß, F. Fritzsch, and A. Bäcker, Chaotic Resonance Modes in Dielectric Cavities: Product of Conditionally Invariant Measure and Universal Fluctuations, Phys. Rev. Lett. **129**, 193901 (2022).
[46] M. You, D. Sakakibara, K. Makino, Y. Morishita, K. Matsumura, Y. Kawashima, M. Yoshikawa, M. Tonosaki, K. Kanno, A. Uchida *et al.*, Universal single-mode lasing in fully chaotic billiard lasers, Entropy **24**, 1648 (2022).
[47] M. Robnik, Classical dynamics of a family of billiards with analytic boundaries, J. Phys. A **16**, 3971 (1983).
[48] J. Wiersig and M. Hentschel, Combining Directional Light Output and Ultralow Loss in Deformed Microdisks, Phys. Rev. Lett. **100**, 033901 (2008).
[49] H. R. Dullin and A. Bäcker, About ergodicity in the family of limaçon billiards, Nonlinearity **14**, 1673 (2001).
[50] M. V. Berry, Regularity and chaos in classical mechanics, illustrated by three deformations of a circular 'billiard', Eur. J. Phys. **2**, 91 (1981).
[51] S. Bittner, E. Bogomolny, B. Dietz, M. Miski-Oglu, and A. Richter, Experimental observation of localized modes in a dielectric square resonator, Phys. Rev. E **88**, 062906 (2013).

[52] S. Bittner, E. Bogomolny, B. Dietz, M. Miski-Oglu, and A. Richter, Dielectric square resonator investigated with microwave experiments, Phys. Rev. E **90**, 052909 (2014).
[53] Y.-D. Yang and Y.-Z. Huang, Mode characteristics and directional emission for square microcavity lasers, J. Phys. D **49**, 253001 (2016).
[54] See Supplemental Material at http://link.aps.org/supplemental/10.1103/PhysRevLett.131.153801 for a detailed description of laser characterization, measurement of lasing dynamics, wave simulations, calculation of local directionality and structure size, and ray tracing algorithm, which includes Refs. [55,56].
[55] V. F. Lazutkin, The existence of caustics for a billiard problem in a convex domain, Mathematics of the USSR Izvestija **7**, 185 (1973).
[56] J. B. Keller and S. I. Rubinow, Asymptotic solution of eigenvalue problems, Ann. Phys. (N.Y.) **9**, 24 (1960).
[57] S. Bittner, K. Kim, Y. Zeng, Q. J. Wang, and H. Cao, Spatial structure of lasing modes in wave-chaotic semiconductor microcavities, New J. Phys. **22**, 083002 (2020).
[58] L. Ge, Y. D. Chong, and A. D. Stone, Steady-state *ab initio* laser theory: Generalizations and analytic results, Phys. Rev. A **82**, 063824 (2010).
[59] S. F. Liew, L. Ge, B. Redding, G. S. Solomon, and H. Cao, Pump-controlled modal interactions in microdisk lasers, Phys. Rev. A **91**, 043828 (2015).
[60] A. Cerjan, B. Redding, L. Ge, S. F. Liew, H. Cao, and A. D. Stone, Controlling mode competition by tailoring the spatial pump distribution in a laser: A resonance-based approach, Opt. Express **24**, 26006 (2016).
[61] A. Cerjan, S. Bittner, M. Constantin, M. Guy, Y. Zeng, Q. J. Wang, H. Cao, and A. D. Stone, Multimode lasing in wave-chaotic semiconductor microlasers, Phys. Rev. A **100**, 063814 (2019).
[62] I. Daubechies, *Ten Lectures on Wavelets* (Society for Industrial and Applied Mathematics, Philadelphia, 1992).
[63] J.-C. Li, J.-L. Xiao, Y.-D. Yang, and Y.-Z. Huang, Random bit generation based on self-chaotic microlasers with enhanced chaotic bandwidth, arXiv:2301.00111.
[64] M. C. Soriano, J. García-Ojalvo, C. R. Mirasso, and I. Fischer, Complex photonics: Dynamics and applications of delay-coupled semiconductors lasers, Rev. Mod. Phys. **85**, 421 (2013).
[65] M. Sciamanna and K. A. Shore, Physics and applications of laser diode chaos, Nat. Photonics **9**, 151 (2015).
[66] X.-Q. Qi and J.-M. Liu, Photonic microwave applications of the dynamics of semiconductor lasers, IEEE J. Sel. Top. Quantum Electron. **17**, 1198 (2011).
[67] A. Brejnak, M. Gebski, A. K. Sokół, M. Marciniak, M. Wasiak, J. Muszalski, J. A. Lott, I. Fischer, and T. Czyszanowski, Boosting the output power of large-aperture lasers by breaking their circular symmetry, Optica **8**, 1167 (2021).
[68] S. Bittner and M. Sciamanna, Complex nonlinear dynamics of polarization and transverse modes in a broad-area VCSEL, APL Photonics **7**, 126108 (2022).
[69] O. Alkhazragi, M. Dong, L. Chen, D. Liang, T. K. Ng, J. Zhang, H. Bagci, and B. S. Ooi, Modifying the coherence of vertical-cavity surface-emitting lasers using chaotic cavities, Optica **10**, 191 (2023).
[70] S. Bittner, S. Knitter, S. F. Liew, and H. Cao, Random-laser dynamics with temporally modulated pump, Phys. Rev. A **99**, 013812 (2019).